Zero-Compensator Filter for Power Sharing Between Battery/Supercapacitor in a Grid-Connected Photovoltaic System

Abderrahmane ABDELLAH [1], *Djilali TOUMI* [1], *M'hamed LARBI* [1], *Sandrine MOREAU* [2]

[1]Laboratory of Energy Engineering and Computer Engineering (L2GEGI), University of Tiaret, BP P 78 Zaaroura, 14000 Tiaret, Algeria
[2]LIAS Laboratory, University of Poitiers, 2 rue Pierre Brousse, TSA 41105, 86073 Poitiers Cedex, France

abderrahmane.abdellah@univ-tiaret.dz, toumi_dj@yahoo.fr, larbi_mh@yahoo.fr, sandrine.moreau@univ-poitiers.fr

DOI: 10.15598/aeee.v20i2.4321

Article history: Aug 05, 2021; Revised Mar 02, 2022; Accepted Mar 14, 2022; Published Jun 30, 2022.

Abstract. *This paper contributes to the energy management of a Hybrid Energy Storage System (HESS), comprising a lithium-ion battery and Supercapacitors (SCs) for a grid-connected photovoltaic system. In general, an Energy Storage System (ESS) can offset the intermittency of renewable energy. However, ESS can absorb large amounts of energy with slow dynamics, but can only absorb fast dynamics when subjected to high currents, which quickly contributes to their wear. To avoid this, SCs are added to energy storage as a supplement to batteries. There are various methods for power-sharing, including the most common, which uses the Low-Pass Filter (LPF). This article proposes a new technique to distribute power between the battery and the SCs using the zero-compensator filter of the battery regulator. Also, this technique is based on the compensation of the energy dissipated by the battery through the SCs. Besides, the State of Charge (SoC) of the battery is kept within safe boundaries. The proposed technique is compared to the ESS and classical HESS techniques. The simulation results confirmed the efficacy of the proposed method of rapidly restoring the DC-link voltage and improving the battery lifespan. In addition, this technique is adaptable to the stand-alone site, and the AC currents showed good quality.*

Keywords

Battery, energy management, photovoltaic, supercapacitor, zero-compensator filter.

1. Introduction

The increasing demand for energy and the exhaustion of fossil fuels mean the search for alternative sources of clean and sustainable energy. Renewable Energy Sources (RESs), particularly solar and wind sources, could fulfill this expectation [1] and [2]. The PV energy source is privileged in terms of reliability and sustainability and has the advantage of being free and inexhaustible. However, it has an intermittent nature due to the variations of different parameters, such as change of irradiation, humidity, temperature, and partial shading effects, which need to be compensated by an ESS [3]. The ESS for the PV system is mainly carried out by batteries, although other means are possible. Batteries have high specific energy but suffer from low power density, low charge/discharge rates, and slow dynamic response and require fairly restrictive maintenance. Indeed, a battery has a limited lifespan, which is about 1000 cycles in the case of a Lithium-Ion for the number of charge-discharge cycles equivalent to 100 % depth of discharge and is limited in the current [4]. PV applications requiring high power peaks force cells to perform many charges or discharges under high current, thus contributing to their rapid wear. To solve this problem, the HESS is necessary to lessen the strain on the battery during transient regimes. Other types of storage exist, such as SCs, which conversely have low specific energy and high specific power. SCs are expected to become economically profitable in the coming years, have a much

longer life span than batteries (about 100,000 cycles), and are therefore able to relieve batteries by absorbing or providing peak power. In addition, the combination of batteries and SCs has complementary qualities and is an excellent option that can cover a wide range of energy and power requirements [5].

Several works have proposed the hybridization of batteries and SCs for all systems. In [6], a PV system in an isolated site depends on batteries and SCs to store energy. The SC converter is controlled as a constant voltage source to accommodate varying load conditions, and the battery converter is controlled as a constant current source. This strategy has helped to improve battery lifespan. The authors in [7] presented the power management of a grid-connected hybrid power generation system based on PV, Alkaline Electrolyzer (AE), Fuel Cell (FC), and SC. The AE is utilized as a reserve load to absorb the extra energy from the system when the PV power is greater than the load demand. The FC is used as a supplementary power supply to provide energy to the system when the PV power is less than the load demand. The SC is introduced to overcome the DC bus power imbalance due to the slow response of AE and FC. In [8], the authors proposed power management for a standalone hybrid AC/DC microgrid, which consists of multiple PVs, multiple Batteries (BES), a single SC, and a single FC with DC and AC loads. The proposed algorithm depends on a Moving Average Filter (MAF) based multi-time-scale adaptive droop power management system with microgrid supervisory control, which offers a reliable algorithm to operate multiple BESs and PVs in a geographically distributed location. Also, maintaining SoC limits is considered. [9] is concerned with the solar vehicle and presents a system that connects batteries, SCs, and PV. It is demonstrated that the integration of SCs into the energy storage system stabilizes the DC bus voltage, eliminates the effect of peak current on the batteries, reduces the stress on the batteries, and thus increases the life of the batteries.

In these types of systems, the PI controller is usually used, as in the previously mentioned studies, but the converter involved is often the DC-DC converter, which introduces nonlinearity problems. The energy management of Hybrid Power Sources (HPS) including, FC/battery/SC using Model Predictive Control (MPC), is successfully studied in [10]. The proposed MPC method maintains the DC bus voltage according to the reference value and limits the slope of the battery and FC current. Nevertheless, the suggested strategy requires vast mathematical calculations, and SoC management is neglected. In [11], an energy management strategy based on Hybrid Bat Search and Artificial Neural Network (HBSANN) is suggested for DC microgrids with HESS. However, this technique shows a non-instantaneous restoration of the DC bus voltage. One of the main drawbacks of the neural network is the need for large data storage and extensive computational resources. In [12], an adaptive Sliding Mode Control (SMC) is used to control a standalone wind turbine based on a Permanent Magnet Synchronous Generator (PMSG). Although this control strategy has the advantage of being insensitive to model uncertainties and external disturbances, the DC bus voltage is not instantaneous to maintain its reference. Also, the authors neglected to adjust the SoC limits. In [13], a deadbeat-based method for HESS, including SCs and batteries, is proposed in DC microgrids. A current observer is used to eliminate the need for sensors to minimize system costs. However, a static error emerged in the DC link voltage when irradiance and load varied.

The basic idea behind energy management in a HESS is that the battery handles the low-frequency power component, while the SC temporarily supports the high-frequency power component. Several studies are used to split the power among the battery and SC. The authors in [14] suggested a wavelet-fuzzy logic-based frequency decoupling strategy to split the power between battery/SC HESS in a new two-propulsion machine-based powertrain of an electric vehicle. The same power-sharing method is presented in [15] but with a different HESS based on FC/SC. However, the aforesaid control technique requires significant resources and computational time. In [16], a fuzzy logic-based intelligent energy management technique is presented to split energy between a HESS in an electric vehicle. The traction part comprises of a Permanent Magnet Synchronous Motor (PMSM). However, this technique is only limited to the traction phase because the proposed fuzzy logic does not allow charging the battery. The vast majority of HESS, including [17], and [18], presented a LPF to divide the frequency spectrum into two frequency bands to be shared between the two HESS components in both grid-connected and independent PV systems. However, due to the slow dynamics of the battery controller, the effect of uncompensated battery power is noticed in the DC link voltage. For this purpose, [3], [19], and [20] introduced an algorithm to recover the uncompensated power using the SC.

This paper proposes an energy management strategy of a grid-connected PV system with HESS to solve the above drawbacks, although the control strategy is adaptable to remote sites. The fundamental idea of this paper is to replace the LPF with a battery controller zero-compensator filter to share power between the SC and the battery. In addition, the input error of the battery PI controller is used to be compensated by the SC. The stress on the batteries is reduced by giving a slow dynamic to the battery PI controller, so the time con-

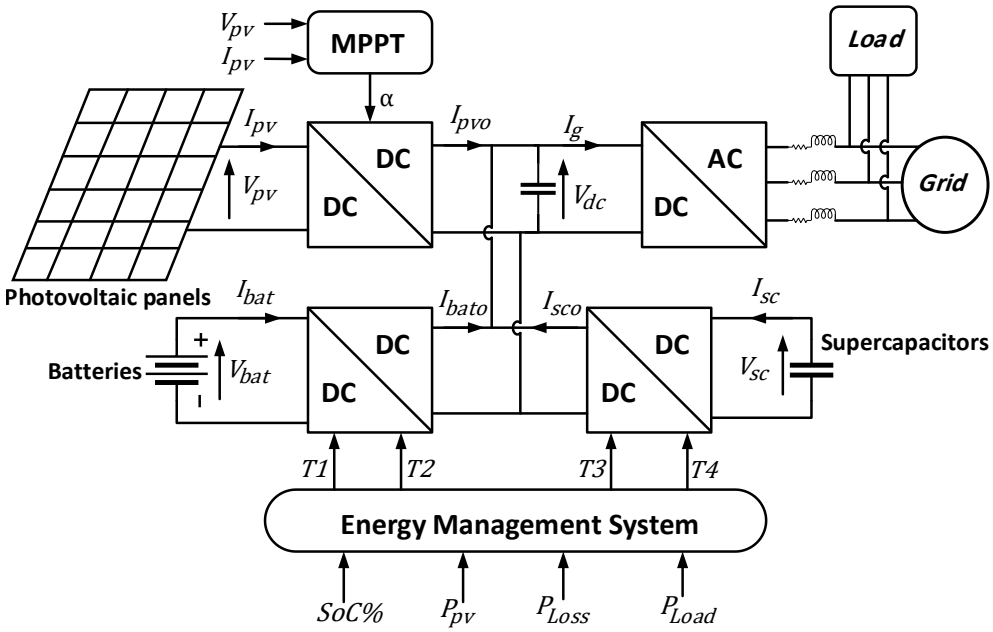

Fig. 1: Block diagram of a grid-connected PV system with HESS.

Nomenclature

HESS	Hybrid Energy Storage System	V_{pv}	Cell output voltage (V)
ESS	Energy Storage System	V_{dc}	DC bus voltage (V)
SC	Supercapacitor	E	Constant voltage (V)
LPF	Low-Pass Filter	E_0	No-load voltage (V)
SoC	State of Charge	V_{Bat}	Battery terminal voltage (V)
PV	Photovoltaic	A_b	Exponential voltage (V)
R_s	Series resistor (Ω)	V_{SC}	SC terminal voltage (V)
R_{sh}	Parallel resistor (Ω)	U_{id}	Inverter d axis voltage component (V)
R_{Bat}	Internal resistance of the battery (Ω)	U_{iq}	Inverter q axis voltage component (V)
R_{SC}	Total internal resistance of the SCs (Ω)	U_{gd}	grid d axis voltage component (V)
R_t	Filter resistance of the grid (Ω)	U_{gq}	grid q axis voltage component (V)
I_{pv}	Cell output current (A)	P_g	Active power (W)
I_{ph}	Cell photocurrent (A)	P_{pv}	PV modules power (W)
I_0	Saturation current (A)	P_{load}	Load power (W)
I_{sc_cell}	Cell short-circuit current (A)	P_{bat}	Battery power (W)
I_{0n}	Reverse saturation current (A)	P_{sc}	SC power (W)
I_{Bat}	Battery current (A)	P_{avg}	Average power (W)
I_{SC}	Total current of the SCs pack (A)	P_{tran}	Transient power (W)
I_{pv}	PV-array current (A)	P_g	Grid power (W)
I_g	DC current of the inverter (A)	Q_g	Reactive Power (Var)
I_{md}	d-axis current coming out of the inverter (A)	τ_{bat}	Time constant of the battery zero-compensator filter (S)
I_{mq}	q-axis current coming out of the inverter (A)	τ_{sc}	Time constant of the SC zero-compensator filter (S)
I_{bat_ref}	Reference current of the battery controller (A)	K_{p_bat}, K_{p_sc}	Battery and SC PI controller's proportional gain
I_{sc_ref}	Reference current of the SC controller (A)	K_{i_bat}, K_{i_sc}	Battery and SC PI controller's Integrator gain
q	Electron charge (C)	C_H	Helmholtz capacitance (F)
Q_c	Cell electric charge (C)	C_{GC}	Gouy-Chapman capacitance (F)
Q_T	Total charge of the SCs pack (C)	C_{dc}	Capacitance of DC bus (F)
T	Cell temperature (K)	L_t	Coupling AC inductor (H)
T_{ref}	Reference temperature (K)	L_{bat}, L_{sc}	I_{Bat} and I_{SC} smoothing inductors (H)
G	Actual irradiation ($W{\cdot}m^{-2}$)	K_b	Polarization constant ($V{\cdot}Ah^{-1}$)
G_n	Nominal irradiation ($W{\cdot}m^{-2}$)	B	Exponential capacity (Ah^{-1})
ϵ_0	Permittivity of free space ($F{\cdot}m^{-1}$)	A_i	Interfacial area between electrodes (m^2)
ϵ	Permittivity of electrolyte material ($F{\cdot}m^{-1}$)	ω_{gr}	Electric angular speed of the grid ($rad{\cdot}S^{-1}$)
$\int idt$	Charge taken/delivered by the battery (Ah)	ω_{nbat}, ω_{nsc}	Battery and SC natural frequency ($rad{\cdot}S^{-1}$)
Q	Maximum ampere-hour capacity	ξ	Damping ratio
C	Molar concentration ($mol{\cdot}m^{-3}$)	N_{s_SC}	Number of SCs connected in series
d	Thickness of Helmholtz layer (m)	N_{p_SC}	Number of SCs connected in parallel
A	Diode ideality factor	K	Boltzmann's constant
K_I	Temperature coefficient	F	Faraday constant
E_g	Band-gap of the semiconductor	R	Ideal gas constant
N_e	Number of electrode layers		

stant of the zero-compensator filter controller automatically increases. The final objectives to be achieved are:

- Efficiency of power-sharing to minimize battery aging by diverting power peaks to the SCs.
- Rapid recovery of the DC bus voltage against sudden changes in irradiation and load.
- Regulation of the battery SoC in a safe limit.
- System independence from the grid when PV and HESS can provide energy.

This work is composed of five sections distributed as follows: Sec. 2. is devoted to the description and global modeling of the system. Section 3. is for controlling the various parts of the system, the power management, and the battery Soc control. The obtained simulations are discussed in Sec. 4. Finally, this article ends with a conclusion summarizing the five sections and main results.

2. System Description

The block diagram of the studied system is presented in Fig. 1. It uses photovoltaic panels as the primary energy source, batteries and supercapacitors as a HESS, and the power grid. The PV array uses the unidirectional DC/DC converter to transport the maximum PV energy to the DC link by employing Maximum Power Point Tracking (MPPT) strategy. The HESS is connected to the DC bus through the buck-boost converters. The energy supplied from the photovoltaic panels and the HESS to the DC bus is transported to the load and the grid via the two-level voltage converter.

The main objective of the proposed PV system with HESS is to supply power to satisfy the load in grid-connected and stand-alone mode while improving the battery life. In this context, SCs are added to the storage system to mitigate the stress on the batteries using a zero-compensating filter-based algorithm. Furthermore, the SoC of the batteries is managed within safe limits. All this is achieved through control commands (T1, T2, T3, T4) sent to the two buck-boost converters. The DC bus presents the link between the DC side and the grid side, so the overall system is stable if the DC bus is kept around its reference. For this, the suggested method also participates in the stabilization of the DC bus voltage by minimizing the disturbances due to the change of irradiation and load. The power management that decides whether the system is operating in stand-alone or grid-connected mode is done by measuring the photovoltaic power, the load power, the losses, and the battery state of charge. The role of the grid connection is to absorb the excess energy when there is a surplus in PV generation, and supply the deficit energy when there is an underproduction of PV energy and discharged batteries.

2.1. Photovoltaic Array Model

Figure 2 presents the "single diode" model of a PV cell, the model is achieved by a series resistor R_s resulting from the contribution of the base and front resistors of the junction and the front and back contacts, and a parallel or shunt resistor R_{sh} coming from the metal contacts and the leakage resistors on the periphery of the cell [21], [22] and [23]. The current-voltage characteristic of a real solar cell is derived from Eq. (1).

$$I_{pv} = I_{ph} - I_0 \left(\exp\left(\frac{q\left(V_{pv} + R_{s \cdot I}\right)}{A \cdot K \cdot T} \right) - 1 \right) + - \frac{V_{pv} + R_s \cdot I_{pv}}{R_{sh}}, \tag{1}$$

where $q = 1.6 \cdot 10^{-16}$ C and $K = 1.3 \cdot 10^{-23}$ J·K^{-1}.

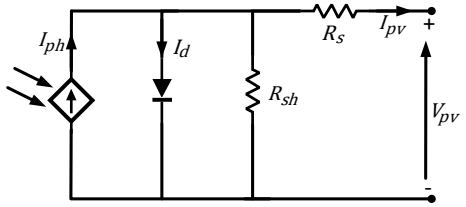

Fig. 2: Equivalent circuit of the photocell.

The current of the PV cell depends directly on the solar irradiance and is proportional to the temperature according to the following equation:

$$I_{ph} = \left(I_{sc\_cell} + K_I \left(T - T_{ref}\right)\right) \frac{G}{G_n}. \tag{2}$$

The equation of the temperature dependence of inverse saturation current of the diode can be expressed by Eq. (3).

$$I_0 = I_{0n} \left(\frac{T_{ref}}{T} \right)^3 \exp\left(\frac{q \cdot E_g}{A \cdot K} \left(\frac{1}{T_{ref}} - \frac{1}{T} \right) \right). \tag{3}$$

A PV module can include sets of cells associated in series and in parallel to produce the necessary voltage and current. The equation for N_p parallel and N_s series of the PV array is given as follows:

$$I_{pv} = N_p I_{ph} - N_p I_0 \cdot \left[\exp\left(q \left(\frac{V_{pv}}{N_s} + \frac{R_s \cdot I_{pv}}{N_p} \right) \cdot \frac{1}{A \cdot K.T} \right) - 1 \right] + - \left(\frac{N_p \cdot V_{pv}}{N_s} + R_s \cdot I_{pv} \right) \frac{1}{R_{sh}}. \tag{4}$$

2.2. Boost Converter Model

The PV array is connected to the DC-bus by using a boost converter represented in Fig. 3. The boost converter is known as a voltage booster. At the first time, the transistor is closed, the current in the inductance increases progressively and gradually as the inductance stores energy until the end of the first period. Then, the transistor opens, and the inductance opposing the current decrease generates a voltage, which is added to the source voltage through the diode.

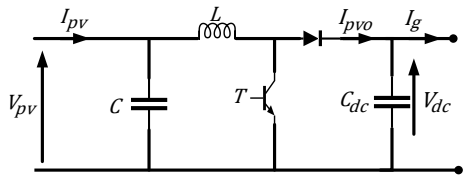

Fig. 3: Circuit diagram of the boost converter.

In average values, the output voltage is a function of the input voltage and the duty cycle. It is expressed in Eq. (5). The regulation of the output voltage is then done by controlling the duty cycle α [24].

$$V_{dc} = \frac{V}{1-\alpha}. \tag{5}$$

2.3. Battery Model

The battery model is available in the MATLAB/Simulink library. This model is simulated using a simple controlled voltage source in series with constant resistance, as illustrated in Fig. 4.

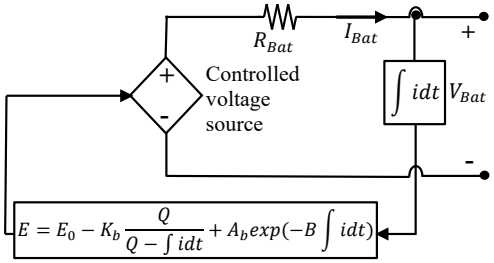

Fig. 4: Mathematical equivalent circuit of the battery.

The battery is modelled as a nonlinear voltage source according to the following equations [11] and [18]:

$$E = E_0 - K_b \frac{Q}{Q - \int idt} + A_b \exp\left(-B \int idt\right), \tag{6}$$

$$V_{Batt} = E - RI_{Batt}. \tag{7}$$

To reach the required nominal current and voltage values, several batteries are interconnected in series-parallel combination.

2.4. Supercapacitor Model

The SC model, as used in this work, is principally based on the Stern principle combination of Helmholtz model and Gouy-Chapman model [11] and [18], which can also be found in the toolbox of MATLAB/Simulink. The schematic diagram of the SC model is shown in Fig. 5.

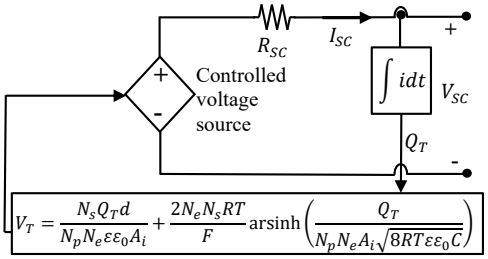

Fig. 5: Mathematical equivalent circuit of SC.

The capacitance of a SC cell is given as follows:

$$C = \left[\frac{1}{C_{GC}} - \frac{1}{C_H}\right], \tag{8}$$

$$C_{GC} = \frac{FQ_C}{2N_e RT} \sinh\left(\frac{Q_C}{N_e^2 A_i \sqrt{8RT\varepsilon\varepsilon_0 C}}\right), \tag{9}$$

$$C_H = \frac{N_e A\ \varepsilon\varepsilon_0}{d} C. \tag{10}$$

In order to reach the required current and voltage values, multiple SCs are connected in series-parallel combination. The total capacitance C_T of the SCs' pack is calculated as:

$$C_T = \frac{N_{p\_SC}}{N_{S\_SC}} C. \tag{11}$$

Considering the resistive losses of the SCs, the output voltage is expressed as follows:

$$V_{SC} = \frac{Q_T}{C_T} - R_{SC} I_{SC}, \tag{12}$$

with

$$Q_T = N_{p\_SC} Q_c \int I_{SC} dt. \tag{13}$$

2.5. Buck-Boost Converter Model

The battery and the SC are linked to the DC bus through two parallel-connected buck-boost converters that provide the energy exchange between this HESS as shown in Fig. 3. To constitute a general model of the buck-boost converter, it is indispensable to examine the buck and boost modes. During boost mode, T1 semiconductor is ON, and T2 is OFF as illustrated in Fig. 6. In this condition, the battery module supplies energy to the DC bus. In buck mode, T2 is ON,

and T1 switches to OFF mode, then the battery receives energy from DC-bus [25]. These sequences are the same for the SC buck-boost converter, i.e., if T3 is turned ON, and T4 goes OFF, the second converter is in boost mode. When T3 becomes OFF, and T4 becomes ON, it is in buck mode.

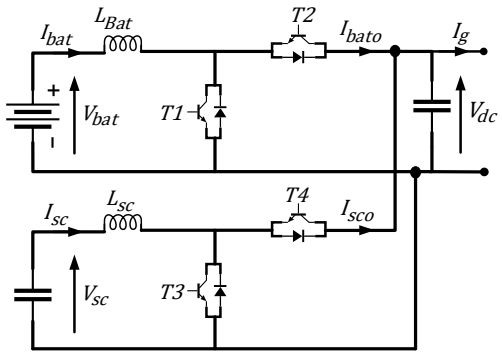

Fig. 6: Circuit diagram of the buck-boost converter.

The analytical models of the two buck-boost converters resulting from the sequence analysis are mentioned in Eq. (14) and Eq. (15).

$$\begin{cases} V_{bat} = \alpha_{bat} V_{dc}, \\ V_{dc} = \dfrac{V_{bat}}{1-\alpha_{bat}}, \end{cases} \tag{14}$$

$$\begin{cases} V_{Sc} = \alpha_{Sc} V_{dc}, \\ V_{dc} = \dfrac{V_{Sc}}{1-\alpha_{Sc}}. \end{cases} \tag{15}$$

2.6. Dc-Link Model

The DC-bus is the capacitor situated between the converters; its function is to maintain a stable continuous voltage and to reduce the ripples. The DC-bus circuit is shown in Fig. 7(A) and its model is expressed by Eq. (16).

$$C_{dc}\frac{V_{dc}}{dt} = I_{pv} \pm I_{bat} \pm I_{sc} - I_g. \tag{16}$$

2.7. Grid Model

From Fig. 7(B), the dynamic model of grid connection in the rotating reference system synchronized with the grid voltage space vector is given by [26]:

$$U_{gd} = -R_f I_{md} - L_f \frac{dI_{md}}{dt} + \omega_{gr} L_f I_{mq} + U_{id}, \tag{17}$$

$$U_{gq} = -R_f I_{mq} - L_f \frac{dI_{mq}}{dt} - \omega_{gr} L_f I_{md} + U_{iq}. \tag{18}$$

3. Control and Power Management

3.1. MPPT Control of PV Module

The Perturb & Observe (P&O) method is one of the most used methods. It is an iterative method to obtain the maximum power point: the characteristics of the PV panel are measured, and then a small disturbance is induced on the voltage (or current) in order to analyze the resulting power variation [27] and [28].

Figure 8 represents the classical algorithm associated with a P&O type MPPT control, where the power evolution is analyzed after each voltage disturbance. For this type of control, two sensors (measuring the current and voltage of the PV panels) are required to determine the PV power at each instant.

3.2. Control of Grid Side Converter

The aims of the grid side converter are to supply energy from the hybrid system side (PV and/or HESS) to the electrical grid and/or load, to control the DC-bus voltage, and to manage reactive power according to the load requirements. Using *d-q* transformation, the active and reactive power are given by:

$$P_g = U_{gd} I_{md} + U_{gq} I_{mq}, \tag{19}$$

$$Q_g = U_{gq} I_{md} - U_{gd} I_{mq}. \tag{20}$$

If the grid voltage vector is oriented with the d axis ($U_{gq} = 0$) [29], the following expression is obtained by:

$$U = U_{gd} + j0. \tag{21}$$

Therefore, Eq. (17) and Eq. (18) may be expressed by:

$$U_{id} = R_f I_{md} + L_f \frac{dI_{md}}{dt} - \omega_{gr} L_f I_{mq} + U, \tag{22}$$

$$U_{iq} = R_f I_{mq} + L_f \frac{dI_{mq}}{dt} + \omega_{gr} L_f I_{md}. \tag{23}$$

The active and reactive power are expressed as follows:

$$P_g = U I_{md}, \tag{24}$$

$$Q_g = -U I_{mq}. \tag{25}$$

According to Eq. (24) and Eq. (25), the active and reactive power can be regulated by *d-q* current components. The control strategy for grid converter is shown in Fig. 7(C).

The control strategy consists of three control loops regulated by the PI controller. These are an external

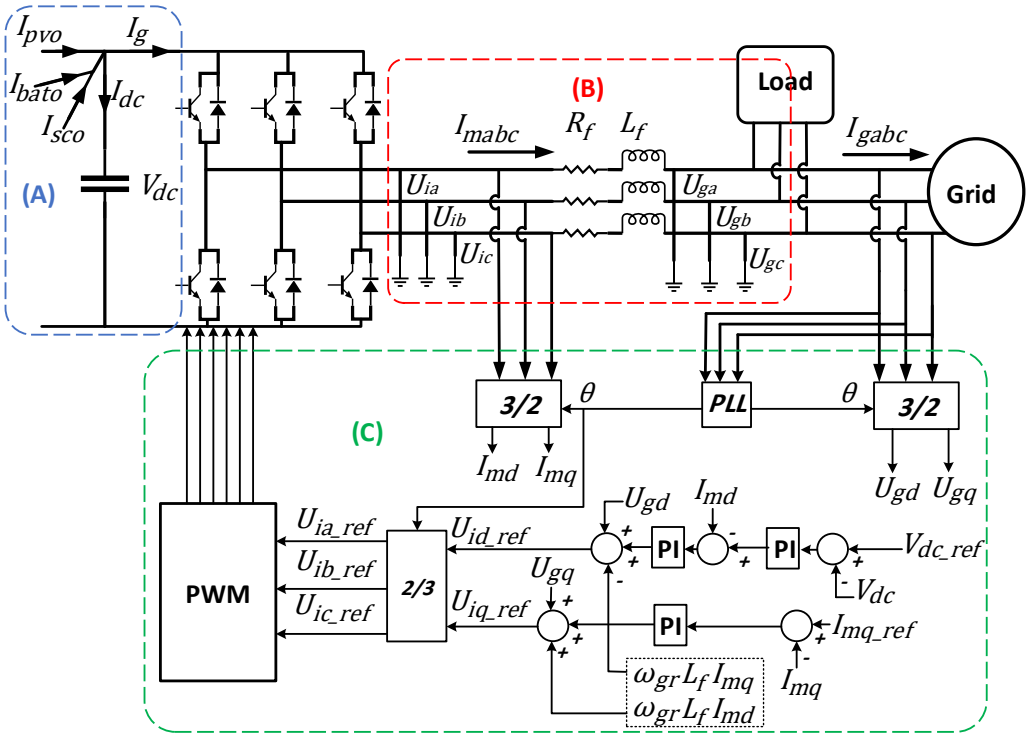

Fig. 7: Diagram of the connection to the grid via a PWM converter: (A) DC bus model, (B) grid model and (C) grid side converter control.

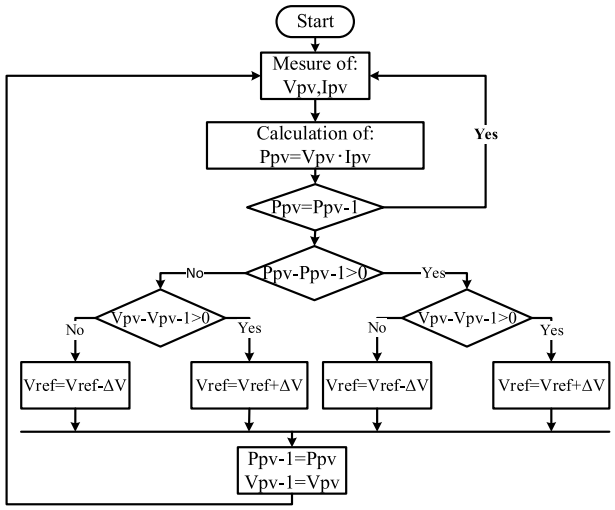

Fig. 8: P&O algorithm.

loop to adjust the DC bus voltage V_{dc} around a reference value V_{dc_ref} and two internal loops to control the active and reactive power by controlling the d-q axis currents. The q-axis current reference signal i_{gq} is generated by the reactive power according to Eq. (25). In addition, the decoupling terms are used, to compensate for the cross-coupling effect due to the relationship between the derivative of the d-axis and q-axis currents. Then, Pulse Width Modulation (PWM) is employed to provide the control signal to regulate the GSC.

3.3. Power Management

Figure 9 presents a new energy sharing technique for a HESS proposed in this article. The main idea of the proposed strategy is that the battery can handle the average power fluctuation, whereas the SC withstands the high-frequency power fluctuations. The total power (P_{tot}) supplied by the HESS is divided into an average power component (P_{avg}) and a transient power component (P_{tran}) using a zero-compensator filter of the battery PI controller. The average power component generated by the zero-compensator filter is sent in the form of a reference current to the buck-boost converter for controlling the battery current. The dynamic power obtained by subtracting the average power component from the total power is sent as a reference current to the current controller of the bidirectional DC-DC converter for SC. The key point of the energy management scheme in a hybrid system is to minimize the stress on the battery, thus extending its lifespan, to preserve the energy balance between the PV module, the HESS system, the utility grid and load all the time, and also to restore the DC bus voltage as quickly as possible.

By considering the power dissipated in the RL filter (P_{loss}); power balance can be expressed as:

$$P_{loss} + P_{loa\ d} - P_{pv} = P_{bat} + P_{sc} = P_{avg} + P_{tran}. \quad (26)$$

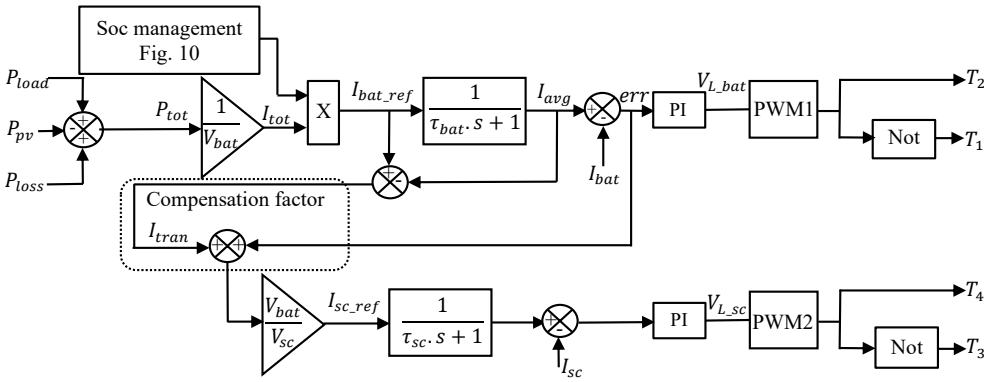

Fig. 9: The proposed power-sharing technique based on a zero-compensator filter for HESS.

The net power required to be provided by the HESS is indicated by the following equation:

$$P_{avg} + P_{tran} = P_{tot} = v_{bat} I_{tot}. \tag{27}$$

This I_{tot} is separated into two components, the low-frequency (average current) and high-frequency (transient current) components. The low-frequency component is given as:

$$I_{avg} = \frac{1}{\tau_{bat} s + 1} I_{tot} = \frac{1}{\tau_{bat} s + 1} I_{bat\_ref}. \tag{28}$$

The I_{avg} is compared to the actual battery current (I_{bat}) and the error (err) is transmitted to the PI controller.

The high-frequency component is given as:

$$I_{tran} = \left(1 - \frac{1}{\tau_{bat} s + 1}\right) I_{bat\_ref}. \tag{29}$$

Due to the slow dynamic of the battery system, the battery may not instantly follow the I_{bat_ref}. Consequently, the uncompensated battery power is:

$$P_{p\_uncomp} = (I_{tran} + err)\, V_{bat}. \tag{30}$$

The SC is also used to compensate the uncompensated battery power, thus increasing the system performances. Therefore, the reference current of SC is given by Eq. (31).

$$I_{SC\_ref} = \frac{P_{p\_uncomp}}{V_{Sc}}. \tag{31}$$

The current I_{sc_ref} is compared to the actual SC current (I_{sc}) and the error is transmitted to the PI controller which goes through the same algorithm as the battery one.

The control signals PWM1 and PWM2 generate switching pulses corresponding to the battery switches (T2 and T1) and the SC switches (T4 and T3).

3.4. SoC Management

The battery SoC is selected between (30–90) % for a longer life cycle. The SoC management strategy for a hybrid system proposed in this article is shown in Fig. 10.

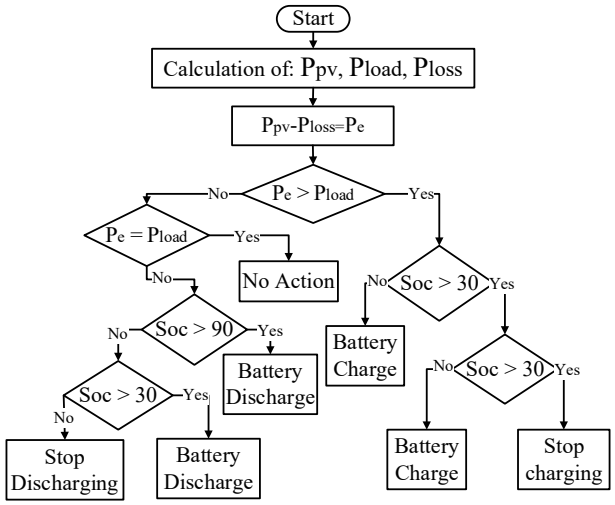

Fig. 10: Flowchart of the battery SoC management.

If the load demand is less than P_e (where $P_e = P_{pv} - P_{loss}$) and if the battery is fully charged, that means that the SoC is equal to 90 %, the PV generator provides the necessary energy to the load and the excess is injected into the grid $P_g = P_e - P_{load}$. Otherwise, for (30 %<SoC<90 %), the average energy surplus between the PV generation and the load power is stored in the battery $P_{bat} = P_{avg} = P_{load} - P_e$. When the load demand is equal to P_e, the PV generator provides the necessary energy only for the load and no action for the battery ($P_{bat} = 0$). If load demand is more than P_e, hence the average power is supplied by the battery when SoC>30 %, otherwise the grid is activated to supply the load even if the PV generation is zero $P_{load} = P_e + P_g$.

3.5. Controller Design

The proposed power management strategy is to estimate the voltage drop across the inductors L_{bat} and L_{sc} to control the currents I_{bat} and I_{sc}. The internal resistance of the inductors is supposed to be negligible. The transfer functions resulting from this control principle are defined by:

$$\begin{cases} G(s) = \dfrac{I_{bat}(s)}{V_{L\_bat}(s)} = \dfrac{1}{L_{bat} \cdot s}, \\ F(s) = \dfrac{I_{sc}(s)}{V_{L\_sc}(s)} = \dfrac{1}{L_{sc} \cdot s}. \end{cases} \tag{32}$$

Using the closed loop transfer function of the HESS (Fig. 11), the transfer functions without filters are obtained from Eq. (33).

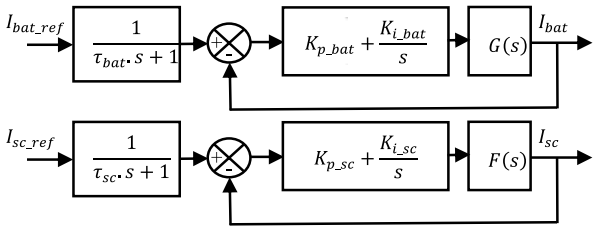

Fig. 11: HESS current control loops.

$$\begin{cases} \mathrm{G}_{cl}(s) = \dfrac{K_{p\_bat} \cdot s + K_{i\_bat}}{L_{bat} \cdot s^2 + K_{p\_bat} \cdot s + K_{i\_bat}} \\ \mathrm{F}_{cl}(s) = \dfrac{K_{p\_sc} \cdot s + K_{i\_sc}}{L_{Sc} \cdot s^2 + K_{p\_sc} \cdot s + K_{i\_sc}} \end{cases}. \tag{33}$$

To ensure dynamic current tracking, the zero-compensator filters (τ_{bat}, τ_{sc}) are used to smooth the desired currents and compensate the zeros of the transfer functions G_{cl} (s) and F_{cl} (s). The resulting transfer functions are given by Eq. (34).

$$\begin{cases} \mathrm{G}_{cl}(s) = \dfrac{1}{\dfrac{L_{bat} \cdot s^2}{K_{i\_bat}} + \dfrac{K_{p\_bat} \cdot s}{K_{i\_bat}} + 1}, \\ \mathrm{F}_{cl}(s) = \dfrac{1}{\dfrac{L_{Sc} \cdot \mathrm{s}^2}{K_{i\_sc}} + \dfrac{K_{p\_sc \cdot s}}{K_{i\_sc}} + 1}, \\ \text{where } \tau_{bat} = \dfrac{K_{p\_bat}}{K_{i\_bat}}, \tau_{Sc} = \dfrac{K_{p\_sc}}{K_{i\_sc}}. \end{cases} \tag{34}$$

The coefficients K_{p_bat} and K_{i_bat} of the battery current corrector are presented by Eq. (35).

$$\begin{cases} K_{p\_bat} = 2.\xi \cdot L_{bat} \cdot \omega_{nbat}, \\ K_{i\_bat} = L_{bat} \cdot \omega_{nbat}^2. \end{cases} \tag{35}$$

The expressions for the coefficients of the SC current corrector are obtained by simply replacing the inductance L_{bat} and the natural frequency ω_{nbat} with the SC current smoothing inductance L_{sc} and the variable ω_{nbat}. The final expressions obtained for this purpose are presented in Eq. (36).

$$\begin{cases} K_{p\_sc} = 2 \cdot \xi \cdot L_{SC} \cdot \omega_{nsc}, \\ K_{i\_sc} = L_{SC} \cdot \omega_{nSC}^2. \end{cases} \tag{36}$$

3.6. Battery Life Extension Strategy

To increase the battery life, the dynamics of the battery current PI controller is reduced to relieve the battery response, especially during transient periods due to intermittent solar production and demand. On the other hand, the dynamics given to the SCs is high to recover the dissipated energy as quickly as possible by using the compensation. The filter time constant τ_{bat} has an important role and defines the dynamics of the system by sharing the total power between the two storage systems. So, reducing the dynamics increases the value of the time constant. However, increasing τ_{bat} improves the smoothing of the battery current, and the SCs will generate and absorb the necessary transient energy as quickly as possible. Therefore, the system is independent of the grid by stabilizing the DC bus.

4. Simulation Results and Discussion

All the sources and associated converters, as well as their local control, have been simulated in the MATLAB/Simulink environment. The results presented below are obtained with the configuration shown in Tab. 1. The reference of the DC bus voltage is adjusted to 630 V, the power is injected into a balanced three-phase network of 220 V, 50 Hz. Conventional PIs are integrated to regulate the various parts of the system, including the HESS current through the buck-boost converters, the DC bus voltage, and the active and reactive power through the two-level inverter. The PI controller gains for the proposed and conventional HESS are listed in Tab. 2.

To examine all possible cases of energy management, the solar irradiation profile and that of the required load are presented in Fig. 12 and Fig. 13 respectively. It is assumed that the SoC has almost reached the 30 % threshold by setting it at 30.1 %. In this regard, the simulation scenarios are detailed below:

- From 0 to 15 s: high generation (1200 W·m^{-2}) equivalent to 6.2 kW, and low demand (1 kW).

Tab. 1: System parameters.

PV array parameters	Value (units)
Open-circuit voltage (v_{oc})	43.2 (V)
Short-circuit current (I_{sc})	5.1 (A)
MPPT voltage (v_{mppt})	34.4 (V)
MPPT current (I_{mppt})	4.8 (A)
MPPT power (P_{mppt})	165 (W)
Cells in series (N_s)	8
Cells in parallel (N_p)	4
Battery parameters	Value (units)
Type	Lithium
Terminal voltage (v_{bat})	12 (V)
Ah capacity	100 (Ah)
Internal resistance (at 25° C)	1.2 (mΩ)
Number of batteries in series	25
Sc parameters	Value (units)
Type	Maxwell BCAP0350-15
Maximum voltage (v_{sc})	2.5 (V)
Nominal capacity	350 (F)
Internal resistance (at 25° C)	3.2 (mΩ)
Number of SCs in series	120
DC-DC coverters parameters	Value (units)
L_{pv}	10 (mH)
L_{bat}	8 (mH)
L_{sc}	8 (mH)
C_{dc}	1 (mF)
Utility grid parameters	Value (units)
L_f	20 (mH)
R_f	2.89 (Ω)
Grid voltages	380/220 (V), 50 (Hz)

Tab. 2: The PI controller parameters.

	HESS	ESS
Battery	$K_{p\_bat} = 0.0213$ $K_{i\_bat} = 0.0284$ $\tau_{bat} = 0.75$ (s)	$K_{p\_bat} = 7.109$ $K_{i\_bat} = 3.158 \cdot 10^3$ $\tau_{bat} = 0.0023$ (s)
Sc	$K_{p\_sc} = 27.368$ $K_{i\_sc} = 4.681 \cdot 10^4$ $\tau_{sc} = 5.846 \cdot 10^{-4}$ (s)	
Grid	$K_{p\_vdc} = 0.351$ $K_{i\_vdc} = 106.082$ $K_{p\_igdq} = 8.67$ $K_{i\_igdq} = 1.253 \cdot 10^3$	

- From 15 to 30 s: generation and demand are equal (1 kW).
- From 30 s due to the low generation (1 kW) the battery is discharged up to 30 %, approximately 60 s.
- From 60 to 80 s: low generation (200 W·m^{-2}) equivalent to 1 kW, and high demand (6 kW).
- From 80 to 100 s: medium generation (1000 W·m^{-2}) equivalent of 5.28 kW, and high demand (6 kW).

In order to inspect the effectiveness of the proposed technique, a comparative study has been performed between ESS, proposed, and classical HESS. The behavior of the battery current with and without supercapacitor is shown in Fig. 14. The ESS battery current response is fast, and significant spikes also appeared

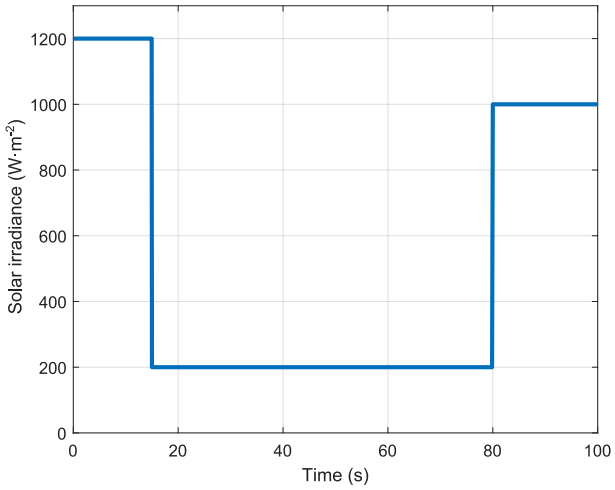

Fig. 12: Solar irradiance profile.

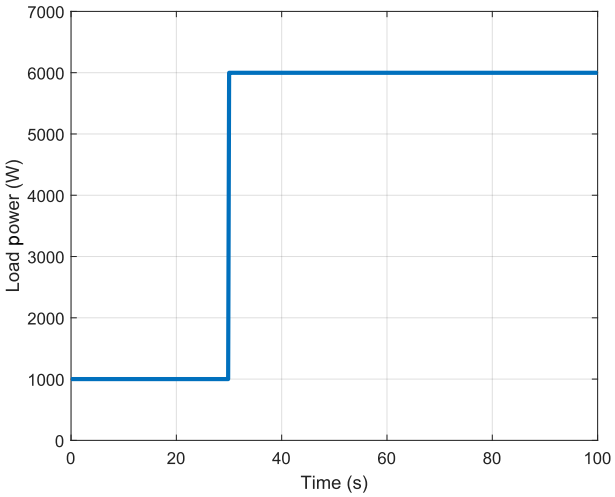

Fig. 13: AC load profile.

when changing solar irradiance or load (at 0 s, 15 s, and 30 s). Because the dynamic given to this system is very high in this case $\tau_{bat} = 0.0023$ s, and also this filter lets through the high-frequency components (below 435 Hz), which will reduce the battery lifespan. On the other hand, from the same figure for the HESS (proposed and classical), it is obvious that with a high time constant value ($\tau_{bat} = 0.75$ s), the battery currents are smoother than the case of ESS. Hence this filter value prevented high-frequency components from passing (above 1.3 Hz). Figure 15 illustrates the comparison of the battery SoC for the three cases. The SoC of the ESS case first reaches the 30 % threshold at 63.6 s, then the SoC of the batteries in HESS (conventional and proposed) reaches it at 63.8 and 64 s respectively, and there is a small decrease below the threshold value concerning the HESS cases, this is due to the exponential shape of the filter that the current takes longer to reach zero as shown in the zoom of Fig. 14. Figure 16 represents the SC currents concerning the two cases of the HESS. The SCs absorb and

deliver the total transient currents with the error component related to the required load peaks and the sudden changes in PV power, and then the SC current slowly returns to zero. Figure 17 shows the SCs SoC of the proposed HESS. The SCs charge or discharge to recover the excess or provide the deficit of energy.

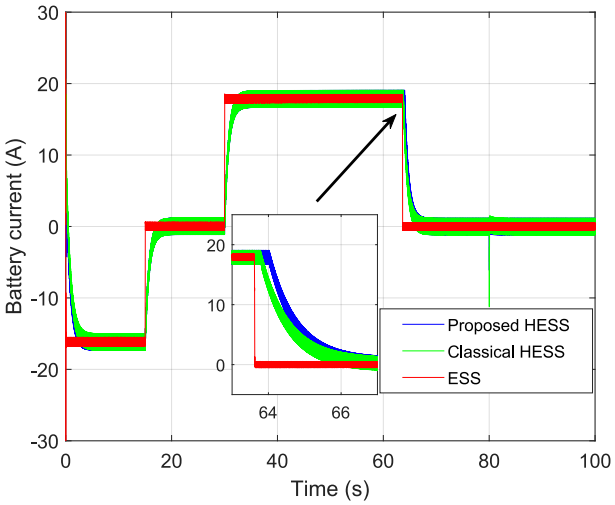

Fig. 14: Battery currents.

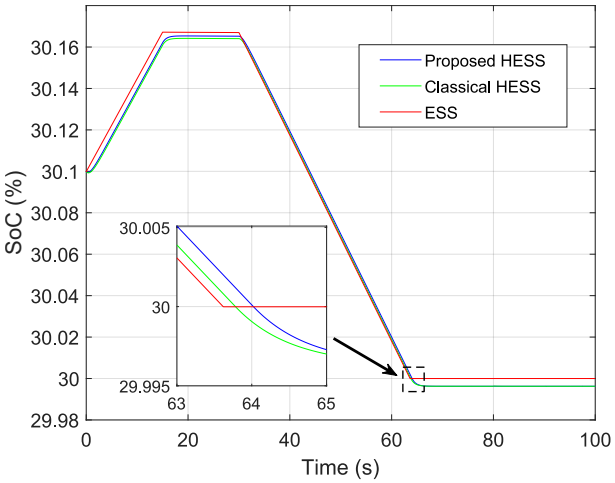

Fig. 15: Battery SoCs.

The DC bus voltage is held around its reference (630 V) without error, as shown in Fig. 18. From 0 to 0.02 s, the proposed HESS has a faster rise time (25 ms) than the ESS and conventional HESS of 30 ms and 52 ms, respectively. During the disturbances, which are illustrated in the zooms, the proposed method shows smaller overshoots of 4 % within the allowed standard range of ±5 % (31.5 V), and takes only 40 ms to reach 630 V. Hence, the zero-compensator filter provides the necessary transient power that the supercapacitors need to stabilize the DC bus as quickly as possible.

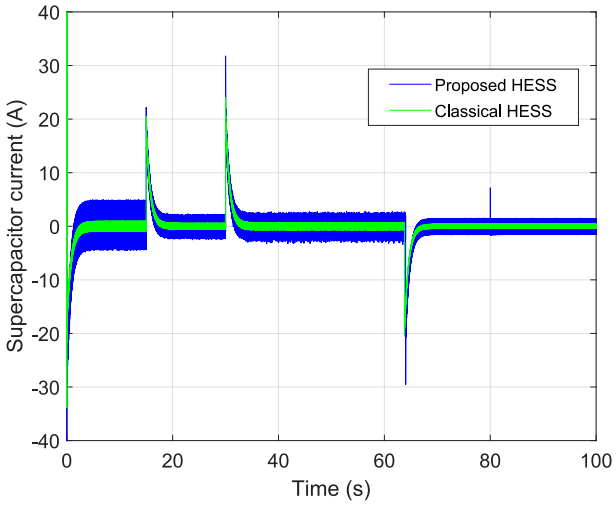

Fig. 16: SC currents.

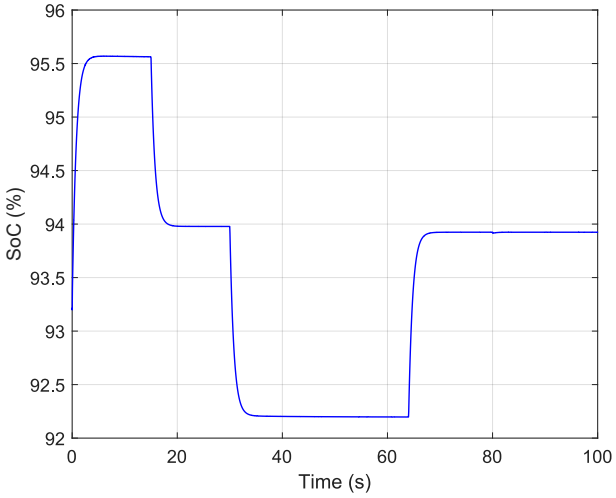

Fig. 17: SC SoC.

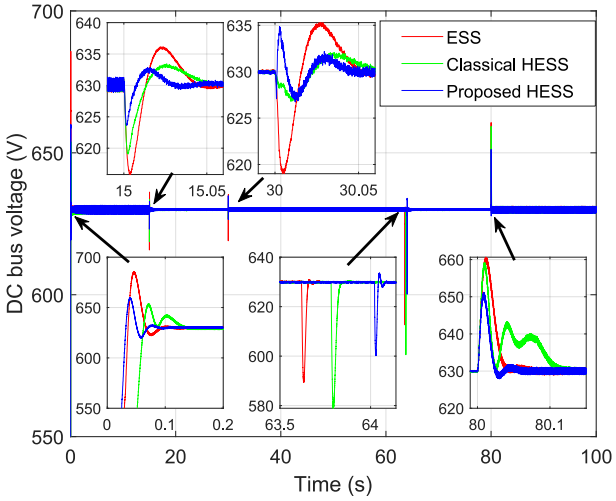

Fig. 18: DC-bus voltages.

Figure 19 represents the management powers in the proposed HESS, it contains four states detailed as follows:

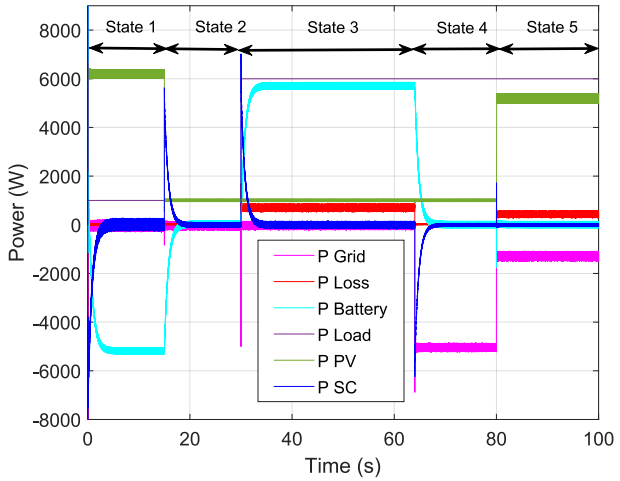

Fig. 19: The powers of the proposed technique.

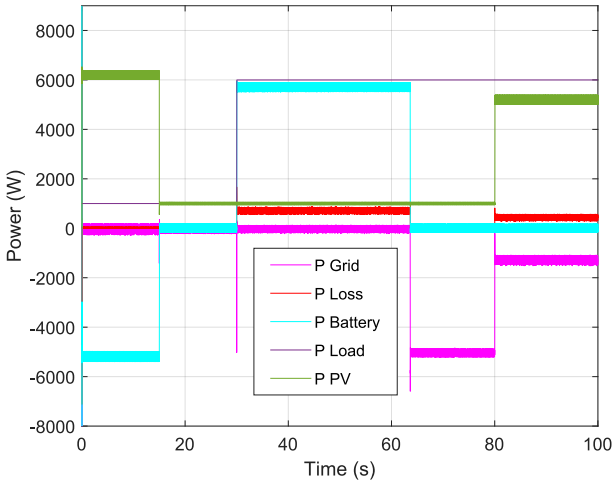

Fig. 20: The powers of the ESS.

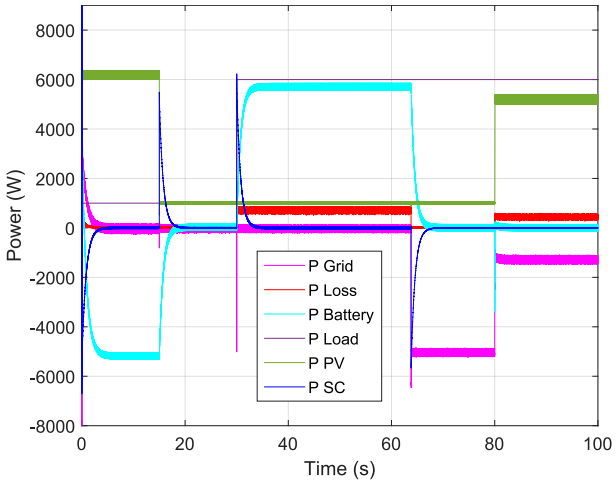

Fig. 21: The powers of the classical technique.

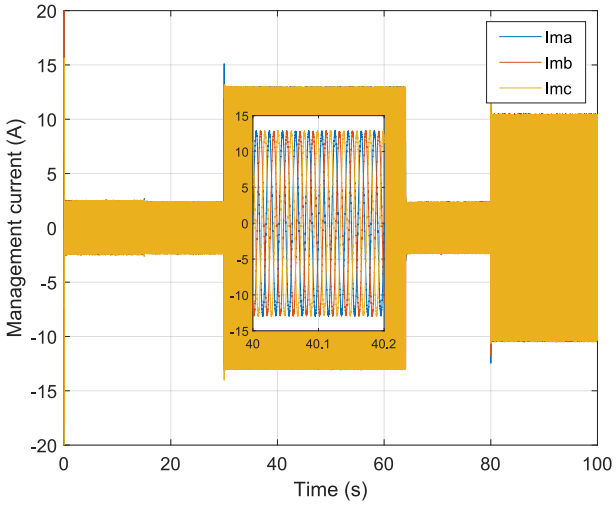

Fig. 22: The output currents of the PWM converter.

State 1: When the power of the PV generation is greater than that of the load, the excess power is distributed over the battery and the SCs.

State 2: The PV generation and the load are equal. As a result, the power difference is zero, causing the battery to switch from charging mode to no-action mode. The SCs provide the high-frequency components to compensate for the smooth shape of the battery at 15 s.

State 3: In the under-generation scenario, the power deficit is supplied by the battery. As for the SCs, they supply the transient peaks at 30 s to meet the load demand. Some losses occurred due to the increase of the current passing through the R-L filter. This state and the two previous ones operate in stand-alone mode.

State 4: When the SoC reaches 30 %, the battery power is zero to protect it against deep discharge. In this scenario, the grid intervenes to compensate for the power deficit. SCs are recharged by high frequencies.

State 5: Grid power decreases due to the increase in PV power to satisfy load requirements. Battery and SC power remain zero, except for small peaks.

Figure 22 represents the management powers in the case of ESS. This technique yields satisfactory results as the proposed HESS, but the battery is forced by high frequencies of the transient regimes, which will decrease its lifespan. Figure 21 demonstrates conventional HESS management. The disadvantage of this technique lies only in system start-up due to the grid intervention to compensate the energy dissipated by the battery for maintaining the DC bus voltage.

To test the effect of the time constant τ_{bat}, the system is subjected to a fluctuating load, with a constant PV power of 1000 W, as shown in Fig 24. Each value of τ_{bat} depends on the dynamics of the PI controller by varying the value of ω_{nbat}. The lower the value of ω_{nbat}, the higher the value of the time constant and vice

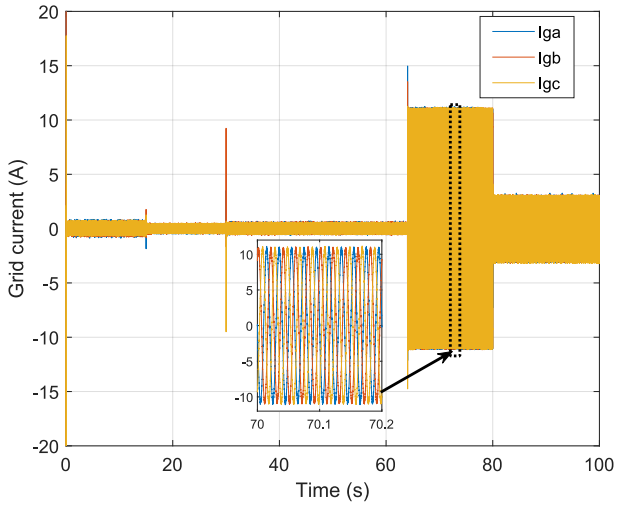

Fig. 23: The grid currents.

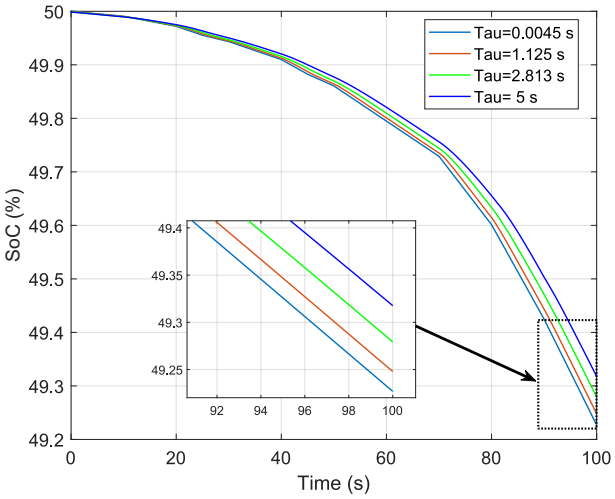

Fig. 25: Battery SoC for different time constants.

versa. Figure 25 shows the battery SoC for different values of τ_{bat}. It can be observed that increasing this value provides considerable relief to the battery, thus increasing its life. It also shows an increasing difference in the SoC over time between the four-time constants.

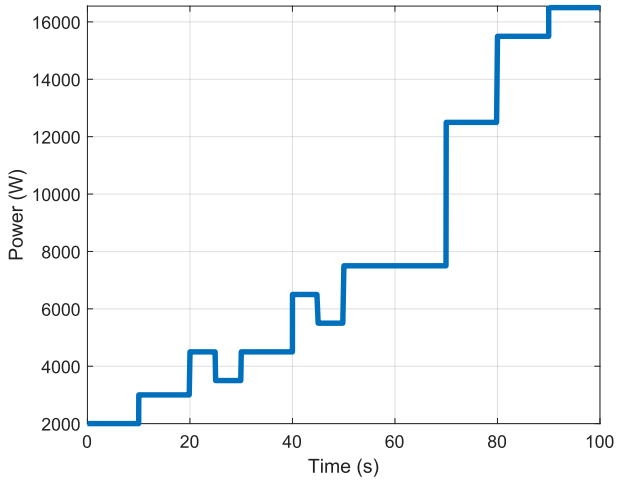

Fig. 24: Fluctuating AC Load profile.

5. Conclusion

This study is based on the energy management of a grid-connected photovoltaic system, which comprises a HESS. The different parts of the overall system, including the PV system, the HESS and the grid, are modeled and controlled. The combination of battery and SC improves the overall battery performance in terms of lifespan and autonomy. The battery controller's zero-compensator filter is implemented to ensure power-sharing of the HESS in different scenarios. This frequency sharing of the power flows is characterized by the time constant τ_{bat}. The proposed technique allows batteries to handle the permanent power component and SCs to deal with the transient power component. The simulation results showed the efficiency of the proposed power-sharing method which, is characterized by: simplicity of implementation, fast stabilization of the DC bus, reduced stress on the battery. In addition, the power management ensures that the battery SoC is controlled within safe limits and allows the system to operate in stand-alone and grid-connected mode with good quality AC.

Author Contributions

A.A. conceptualized the ideas, designed the models and wrote the manuscript. D.T. contributed to the design of the research and helped to carry out the hybrid energy storage system control. M.L. analyzed the results and contributed to the interpretation. Both D.T. and M.L. involved in planning and supervised the work. S.M. provided feedback and made necessary corrections.

References

[1] OUNNAS, D., D. GUIZA, Y. SOUFI and M. MAAMRI. Design and Hardware Implementation of Modified Incremental Conductance Algorithm for Photovoltaic System. *Advances in Electrical and Electronic Engineering*. 2021, vol. 19, iss. 2, pp. 100–111. ISSN 1804-3119. DOI: 10.15598/aeee.v19i2.3881.

[2] ABDELLAH, A., D. TOUMI and M. LARBI. Second-Order Super-Twisting Control of an Autonomous Wind Energy Conversion System Based on PMSG for Robustness and Chattering Elim-

ination. In: *Proceedings of the 4th International Conference on Electrical Engineering and Control Applications*. Singapore: Springer Singapore, 2021, pp. 579–594. ISBN 978-981-15-6403-1. DOI: 10.1007/978-981-15-6403-1_39.

[3] MANANDHAR, U., N. R. TUMMURU, S. K. KOLLIMALLA, A. UKIL, G. H. BENG and K. CHAUDHARI. Validation of Faster Joint Control Strategy for Battery- and Supercapacitor-Based Energy Storage System. *IEEE Transactions on Industrial Electronics*. 2018, vol. 65, iss. 4, pp. 3286–3295. ISSN 1557-9948. DOI: 10.1109/TIE.2017.2750622.

[4] KHALIGH, A. and Z. LI. Battery, Ultracapacitor, Fuel Cell, and Hybrid Energy Storage Systems for Electric, Hybrid Electric, Fuel Cell, and Plug-In Hybrid Electric Vehicles: State of the Art. *IEEE Transactions on Vehicular Technology*. 2010, vol. 59, iss. 6, pp. 2806–2814. ISSN 1939-9359. DOI: 10.1109/TVT.2010.2047877.

[5] KRIM, Y., D. ABBES, S. KRIM and M. F. MIMOUNI. A flexible control strategy of a renewable active generator to participate in system services under grid faults. *International Transactions on Electrical Energy Systems*. 2019, vol. 29, iss. 1, pp. 1–24. ISSN 2050-7038. DOI: 10.1002/etep.2687.

[6] MAHESWARI, L., P. S. RAO, N. SIVAKUMARAN, G. S. ILANGO and C. NAGAMANI. A control strategy to enhance the life time of the battery in a stand-alone PV system with DC loads. *IET Power Electronics*. 2017, vol. 10, iss. 9, pp. 1087–1094. ISSN 1755-4543. DOI: 10.1049/iet-pel.2016.0735.

[7] KONG, L., J. YU and G. CAI. Modeling, control and simulation of a photovoltaic /hydrogen/ supercapacitor hybrid power generation system for grid-connected applications. *International Journal of Hydrogen Energy*. 2019, vol. 44, iss. 46, pp. 25129–25144. ISSN 0360-3199. DOI: 10.1016/j.ijhydene.2019.05.097.

[8] SHARMA, R. K. and S. MISHRA. Dynamic Power Management and Control of a PV PEM Fuel-Cell-Based Standalone ac/dc Microgrid Using Hybrid Energy Storage. *IEEE Transactions on Industry Applications*. 2018, vol. 54, iss. 1, pp. 526–538. ISSN 1939-9367. DOI: 10.1109/TIA.2017.2756032.

[9] CABRANE, Z., D. BATOOL, J. KIM and K. YOO. Design and simulation studies of battery-supercapacitor hybrid energy storage system for improved performances of traction system of solar vehicle. *Journal of Energy Storage*. 2020, vol. 32, iss. 1, pp. 1–13. ISSN 2352-152X. DOI: 10.1016/j.est.2020.101943.

[10] AMIN, R. T. BAMBANG, A. S. ROHMAN, C. J. DRONKERS, R. ORTEGA and A. SASONGKO. Energy Management of Fuel Cell/Battery/Supercapacitor Hybrid Power Sources Using Model Predictive Control. *IEEE Transactions on Industrial Informatics*. 2014, vol. 10, iss. 4, pp. 1992–2002. ISSN 1941-0050. DOI: 10.1109/TII.2014.2333873.

[11] SINGH, P. and J. S. LATHER. Dynamic power management and control for low voltage DC microgrid with hybrid energy storage system using hybrid bat search algorithm and artificial neural network. *Journal of Energy Storage*. 2020, vol. 32, iss. 1, pp. 1–12. ISSN 2352-152X. DOI: 10.1016/j.est.2020.101974.

[12] KORD, H. and S. M. BARAKATI. Design an adaptive sliding mode controller for an advanced hybrid energy storage system in a wind dominated RAPS system based on PMSG. *Sustainable Energy, Grids and Networks*. 2020, vol. 21, iss. 1, pp. 1–12. ISSN 2352-4677. DOI: 10.1016/j.segan.2020.100310.

[13] WANG, B., U. MANANDHAR, X. ZHANG, H. B. GOOI and A. UKIL. Deadbeat Control for Hybrid Energy Storage Systems in DC Microgrids. *IEEE Transactions on Sustainable Energy*. 2019, vol. 10, iss. 4, pp. 1867–1877. ISSN 1949-3037. DOI: 10.1109/TSTE.2018.2873801.

[14] DUSMEZ, S. and A. KHALIGH. A Supervisory Power-Splitting Approach for a New Ultracapacitor–Battery Vehicle Deploying Two Propulsion Machines. *IEEE Transactions on Industrial Informatics*. 2014, vol. 10, iss. 3, pp. 1960–1971. ISSN 1941-0050. DOI: 10.1109/TII.2014.2299237.

[15] ERDINC, O., B. VURAL, M. UZUNOGLU and Y. ATES. Modeling and analysis of an FC/UC hybrid vehicular power system using a wavelet-fuzzy logic based load sharing and control algorithm. *International Journal of Hydrogen Energy*. 2009, vol. 34, iss. 12, pp. 5223–5233. ISSN 0360-3199. DOI: 10.1016/j.ijhydene.2008.10.039.

[16] SELLALI, M., S. ABDEDDAIM, A. BETKA, A. DJERDIR, S. DRID and M. TIAR. Fuzzy-Super twisting control implementation of battery/super capacitor for electric vehicles. *ISA Transactions*. 2019, vol. 95, iss. 1, pp. 243–253. ISSN 0019-0578. DOI: 10.1016/j.isatra.2019.04.029.

[17] KRISHAN, O. and S. SUHAG. Grid-independent PV system hybridization with fuel cell-battery/supercapacitor: Optimum sizing and comparative techno-economic analysis. *Sustainable Energy Technologies and Assessments*. 2020, vol. 37, iss. 1, pp. 1–17. ISSN 2213-1388. DOI: 10.1016/j.seta.2019.100625.

[18] ARGYROU, M. C., C. C. MAROUCHOS, S. A. KALOGIROU and P. CHRISTODOULIDES. A novel power management algorithm for a residential grid-connected PV system with battery-supercapacitor storage for increased self-consumption and self-sufficiency. *Energy Conversion and Management*. 2021, vol. 246, iss. 1, pp. 1–18. ISSN 0196-8904. DOI: 10.1016/j.enconman.2021.114671.

[19] PUNNA, S., U. B. MANTHATI and A. C. RAVEENDRAN. Modeling, analysis, and design of novel control scheme for TWO-INPUT bidirectional DC-DC converter for HESS in DC microgrid applications. *International Transactions on Electrical Energy Systems*. 2021, vol. 31, iss. 10, pp. 1–23. ISSN 2050-7038. DOI: 10.1002/2050-7038.12774.

[20] ZHANG, X., D. GAMAGE and A. UKIL. Rising and falling edge compensation based faster control strategy for hybrid energy storage system in PV microgrid. *Electric Power Systems Research*. 2021, vol. 190, iss. 1, pp. 1–10. ISSN 0378-7796. DOI: 10.1016/j.epsr.2020.106856.

[21] BHUKYA, K. N., K. CHATTERJEE and T. K. CHATTERJEE. Assessment of MPPT Techniques During the Faulty Conditions of PV System. *Advances in Electrical and Electronic Engineering*. 2018, vol. 16, iss. 1, pp. 15–24. ISSN 1804-3119. DOI: 10.15598/aeee.v16i1.2581.

[22] KEDARI, S., R. VERAMALLA and A. KODAKKAL. Optimized Gains for the Control of Islanded Solar Photovoltaic and Wind System. *Advances in Electrical and Electronic Engineering*. 2021, vol. 19, iss. 4, pp. 295–303. ISSN 1804-3119. DOI: 10.15598/aeee.v19i4.4227.

[23] MERAL, M. E. and D. CELIK. DSOGI-PLL Based Power Control Method to Mitigate Control Errors Under Disturbances of Grid Connected Hybrid Renewable Power Systems. *Advances in Electrical and Electronic Engineering*. 2018, vol. 16, iss. 1, pp. 81–91. ISSN 1804-3119. DOI: 10.15598/aeee.v16i1.2485.

[24] EYDI, M., S. I. H. SABZEVARI and R. GHAZI. A Novel Strategy of Maximum Power Point Tracking for Photovoltaic Panels Based on Fuzzy Logic Algorithm. *Advances in Electrical and Electronic Engineering*. 2020, vol. 18, iss. 1, pp. 1–10. ISSN 1804-3119. DOI: 10.15598/aeee.v18i1.3511.

[25] CAMARA, M. B., B. DAKYO and H. GUALOUS. Polynomial Control Method of DC/DC Converters for DC-Bus Voltage and Currents Management—Battery and Supercapacitors. *IEEE Transactions on Power Electronics*. 2012, vol. 27, iss. 3, pp. 1455–1467. ISSN 1941-0107. DOI: 10.1109/TPEL.2011.2164581.

[26] REHMAN, A. U., Z. W. KHAN, B. REHMAN, S. IQBAL and M. GUL. Study on Dynamic Characteristics of UHVDC System under Hierarchical Infeed Mode with STATCOM. *Advances in Electrical and Electronic Engineering*. 2021, vol. 19, iss. 1, pp. 16–27. ISSN 1804-3119. DOI: 10.15598/aeee.v19i1.3937.

[27] LATKOVA, M., M. BAHERNIK, M. HOGER and P. BRACINIK. FSM Model of a Simple Photovoltaic System. *Advances in Electrical and Electronic Engineering*. 2015, vol. 13, iss. 3, pp. 230–235. ISSN 1804-3119. DOI: 10.15598/aeee.v13i3.1411.

[28] DEPURU, S. R. and M. MAHANKALI. Boost Converter Fed High Performance BLDC Drive for Solar PV Array Powered Air Cooling System. *Advances in Electrical and Electronic Engineering*. 2017, vol. 15, iss. 2, pp. 154–168. ISSN 1804-3119. DOI: 10.15598/aeee.v15i2.2133.

[29] ABOUDRAR, I., S. EL HANI, H. MEDIOUNI and A. AGHMADI. Modeling and Robust Control of a Grid Connected Direct Driven PMSG Wind Turbine By ADRC. *Advances in Electrical and Electronic Engineering*. 2018, vol. 16, iss. 4, pp. 402–413. ISSN 1804-3119. DOI: 10.15598/aeee.v16i4.2952.

About Authors

Abderrahmane ABDELLAH was born in Tiaret, Algeria, in 1992. He received his M.Sc. degree in Electrical Engineering from the University of Tiaret, Algeria, in 2016, where he is presently working towards his Ph.D. degree in the L2GEGI Laboratory. His current research interests include microgrids, energy management, hybrid storage system, multilevel inverters, power electronics, and faults diagnosis.

Djilali TOUMI graduated with his Ph.D. degree in from the National Polytechnic School of Algiers in Algeria. He is actually a professor in the Electrical Engineering Department at the University of Tiaret

in Algeria. His current research interests include advanced techniques in electrical system control and diagnosis with intelligent algorithms.

M'hamed LARBI was born in Algeria in 1968. He received the Ph.D. degree in 2011 from the University of Science and Technology of Oran USTO Algeria. Since 2019 he was a professor at the University of Tiaret-Algeria. His research interests lie in the diagnosis and robust control of Electrical Machines drives.

Sandrine MOREAU was born in France in 1972. She received her Ph.D. degree from the University of Poitiers in automatic control in 1999. She is now professor at the University of Poitiers (France). Her research interests are; modelling, identification, diagnosis and control of electrical machines associated with static converters.